AIAA JOURNAL
Vol. 30, No. 6, June 1992

Axially Symmetric Pulse Propagation in Semi-Infinite Hollow Cylinders

T. Kohl* and S. K. Datta†
University of Colorado, Boulder, Colorado 80309
and
A. H. Shah‡
University of Manitoba, Winnipeg, Manitoba R3T 2N2, Canada

The effects of dispersion and end conditions on axially symmetric pulse propagation in semi-infinite tubes are investigated. Numerical modeling of the dynamic response is accomplished using a stable and efficient finite element and wave propagation based method. This method yields the dispersive and modal data required to express displacements in a frequency domain modal expansion. Boundary conditions are applied to the tube end to obtain mode amplitudes. A fast Fourier transform is then used to get the time response. The specific end conditions considered are intended to give some insight into how the tube would behave as a member of a jointed truss structure.

Introduction

AXIALLY symmetric pulse propagation in a composite tube is considered here to explore a method, based on concepts of wave propagation, for ultrasonic nondestructive means for structural verification and health monitoring of large space structure truss assemblies. Although the modeling technique presented is applied here to composite tubes, the method is completely general and may be applied to tubes of other materials. This method has the advantage that it can be used to analyze tubes that are radially inhomogeneous, such as a composite tube with aluminum cladding.

For small deformations of a truss assembly, most of the energy within the deformed structure is associated with the axially symmetric motion of the tube members forming the assembly. In other words, the extension or compression of each tube will dominate the response of the structure, and tube bending will be of lesser importance. In this case, bar modes are predominant in the deformation of each tube in truss structures.

In the present paper, we present a method for obtaining the dynamic response of a semi-infinite tube to prescribed end conditions. The importance of the semi-infinite tube dynamic model is that the response of a finite tube can be determined as a superposition of semi-infinite tube responses. The effect of different end conditions on the dynamic response of semi-infinite composite tubes is considered here. We are primarily interested in the behavior of the tube when its end is jointed, as in a truss assembly. Two types of idealized end conditions are considered: one in which the end is rigid and is given an axial displacement pulse, and the other representing the end in smooth contact with a rigid joint that is given an axial displacement. Thus, in boundary condition I (B.C.I) there are zero radial and circumferential displacements, and in boundary condition II (B.C.II) zero shear stresses σ_{rz} and $\sigma_{\theta z}$ at the tube end will be considered.

The modeling technique combines finite element representation and wave propagation and was proposed by Nelson et al.[1] This method is used to obtain dispersion of guided waves and modes of propagation as discussed in greater detail by Kohl et al.[2] The propagation of disturbance is represented in terms of modes. Boundary conditions are then used to determine the amplitudes of the modes, yielding a frequency domain solution. A fast Fourier transform is then used to obtain the time response. Emphasis will be placed on experimentally measurable quantities, specifically axial strain and radial displacement.

The focus of the present examination is on the determination of the effect of boundary conditions on the modal amplitudes and how this influences the consequent time response. Also examined is the effect of elastic wave dispersion on the observable time domain response of composite tubes.

Governing Equations

The equations governing the propagation of waves in the tube are solved by discretizing the tube in the radial direction, which allows tubes made of laminas with different constitutive relations to be modeled. Reference is made to cylindrical coordinates r, θ, and z (Fig. 1), and the displacement components are u_j ($j = r,\theta,z$). It is assumed that the motion is axially symmetric. Three noded one-dimensional elements in the radial direction with displacement continuity between elements are used so that, within the kth element, the displacement variation is written as

$$\begin{Bmatrix} u_r(r,z,t) \\ u_\theta(r,z,t) \\ u_z(r,z,t) \end{Bmatrix}^{(k)} = [N(r)]\{q(z,t)\}^{(k)} \tag{1a}$$

where

$$\{q(z,t)\}^{(k)T} = [u_{r_b}, u_{\theta_b}, u_{z_b}, u_{r_m}, u_{\theta_m}, u_{z_m}, u_{r_f}, u_{\theta_f}, u_{z_f}] \tag{1b}$$

The subscripts b, m, and f refer to back, middle, and front or inner, middle, and outer nodes of the element, respectively, as shown in Fig. 1a. Matrices and related equations not given explicitly in the text (i.e., $[N(r)]$) can be found in the Appendix. An ordered array of nodal displacement components can be expressed in a frequency domain modal expansion in the form

$$\{q(z,\omega)\} = \sum_{n=1}^{M} A_n \{Q_0(\omega)\}_n e^{-\gamma_n z} \tag{2}$$

where ω is the circular frequency and γ_n the wave numbers.

Received May 13, 1991; revision received Sept. 27, 1991; accepted for publication Sept. 30, 1991. Copyright © 1992 by the American Institute of Aeronautics and Astronautics, Inc. All rights reserved.

*Research Assistant, Department of Mechanical Engineering and Center for Space Construction, Campus Box 427.
†Professor; currently at University of Connecticut, Department of Mechanical Engineering, Storrs, CT 06269.
‡Professor, Department of Civil Engineering.

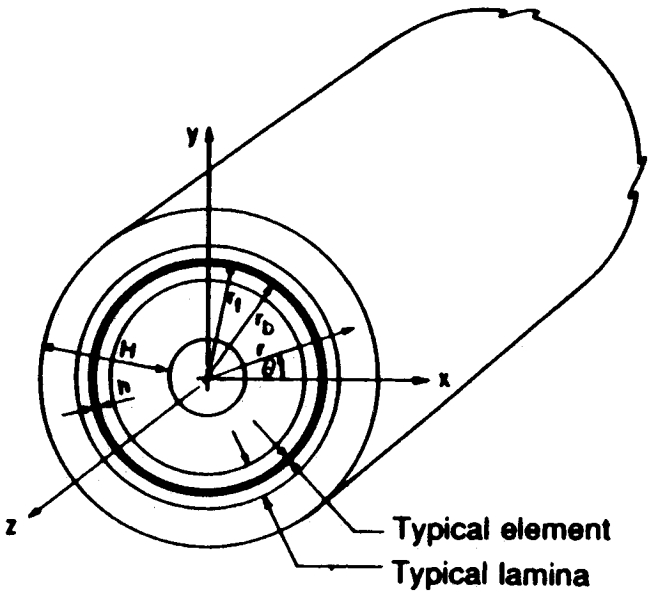

Fig. 1a Element of a laminated cylinder.

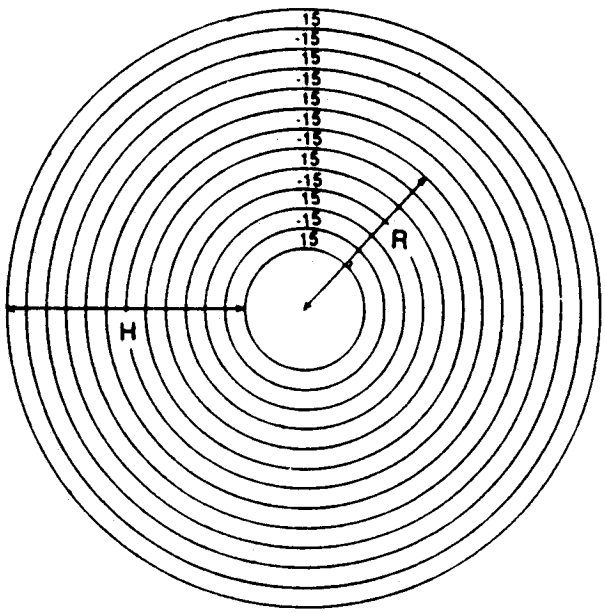

Fig. 1b Tube ply lay-up (not to scale).

The factor $e^{-i\omega t}$ has been suppressed. The vector $\{Q_0\}_n$ is an ordered array of all nodal displacements of the nth mode, and A_n is the amplitude of this mode.

Hamilton's principle is applied to the discretized system, yielding, for specified frequency, a quadratic eigenvalue problem in γ_n:

$$[\gamma_n^2[K_1] - \gamma_n([K_2] - [K_2]^T) - ([K_3] - \omega^2[M])]\{Q_0\}_n = 0 \quad (3)$$

The vector $\{Q_0\}_n$ is the eigenvector associated with the root γ_n. The $[K_i]$ are stiffness related matrices, and $[M]$ is the consistent mass matrix assembled from the respective elemental matrices given in the Appendix. For details, the reader is referred to Kohl et al.[2]

This method for obtaining the modes and wave numbers of the displacement expansion was first proposed by Nelson et al.[1] for tubes with general orthotropic layers and was extended to tubes with general anisotropic layers by Huang and Dong.[3] For fiber-reinforced laminated tubes, layers are general anisotropic if they do not have uniaxial fibers or fiber angles of ± 90 deg. For a more complete derivation of the aforementioned eigenvalue problem and the numerical method in general, the reader is referred to Kohl et al.[2]

The solutions for the eigenvalues γ_n may be real, complex, or imaginary. For the axial dependence given in Eq. (2), imaginary roots are associated with propagating modes, whereas real and complex roots refer to nonpropagating and evanescent modes, respectively. Note that, in the context of most wave propagation literature in which real eigenvalues refer to propagating modes, the eigenvalue γ considered here is related to the wave number ξ according to $\gamma = -i\xi$. The eigenvalues of Eq. (3) always occur in pairs (positive and negative) for real and imaginary roots, and they always occur in foursomes for complex roots.

For a discretized system with P nodes, there are a total of $3P$ degrees of freedom. Solution of the eigenvalue problem [Eq. (3)] yields $6P$ solutions for wave numbers ξ_n and their associated eigenvectors $\{Q_0\}_n$. Considering elastic waves propagating in the direction of increasing axial coordinate, only half of the total solutions or $3P$ solutions are acceptable. Referring to the axial dependence given in Eq. (2), from stability considerations, only complex and real eigenvalues γ_n with positive real parts are admissible. For propagating modes, it is required that the group velocity $d\omega/d\xi$ be positive. The implication of requiring positive group velocity is that the disturbance propagates in the positive axial direction. A further discussion of group velocity will be found later in this paper.

Once the eigenvectors $\{Q_0\}_n$ are known, Eqs. (1a) and (2) may be combined so that the displacement variation within each element can be written as

$$\begin{Bmatrix} u_r(r,z,\omega) \\ u_\theta(r,z,\omega) \\ u_z(r,z,\omega) \end{Bmatrix}^{(k)} = [N(r)] \sum_{n=1}^{M} A_n \{Q_0\}_n^{(k)} e^{-\gamma_n z} \quad (4)$$

where the mode amplitudes A_n are obtained by use of appropriate boundary conditions at $z = 0$.

The first limiting set of boundary conditions for a jointed tube subjected to axial impact is considered here to be entirely displacement based. At the tube end $z = 0$, the radial and circumferential displacements are zero and the axial displacement imposed is considered to be of unit amplitude:

$$\text{B.C.I} \quad \begin{aligned} u_r(r,z=0,\omega) &= 0.0 \\ u_\theta(r,z=0,\omega) &= 0.0 \\ u_z(r,z=0,\omega) &= 1.0 \end{aligned} \quad (5)$$

The linear system derived from this boundary condition and used to solve for the amplitudes A_n is given by

$$\{u\}_{\text{nodal}} = \sum_{n=1}^{M} A_n \{Q_0\}_n \quad (6a)$$

and

$$\{u\}_{\text{nodal}}^T = [u_{r_1}\ u_{\theta_1}\ u_{z_1}\ u_{r_2}\ u_{\theta_2}\ u_{z_2} \cdots u_{r_P}\ u_{\theta_P}\ u_{z_P}]$$

$$= [0\ \ 0\ \ 1\ \ 0\ \ 0\ \ 1\ \cdots\ 0\ \ 0\ \ 1] \quad (6b)$$

where the subscript numbers specify the node number.

The second boundary condition to be considered will include the same uniform axial displacement of unit magnitude together with zero shear stresses, σ_{rz} and $\sigma_{\theta z}$, on the tube end at $z = 0$. This boundary condition must be implemented with some care because there is no guarantee of stress continuity between elements with the method used. A consistent nodal force vector is obtained using a variational principle to satisfy the shear stress free end condition.

Using the axial displacement condition that gives $\delta u_z = 0$, application of the principle of virtual work yields the end condition equation

$$\int_A (\sigma_{\theta z}\delta u_\theta + \sigma_{rz}\delta u_r)\, dA = 0 \quad (7)$$

where δ is the variational operator.

The strains may be expressed in terms of the displacements appearing in Eq. (4) using strain displacement transformation matrices $[a(r)]$ and $[b(r)]$. This gives for the strains in the kth element

$$\{\epsilon\}^{(k)} = [b(r)] \sum_{n=1}^{M} - A_n \gamma_n \{Q_0\}_n^{(k)} e^{-\gamma_n z} + [a(r)] \sum_{n=1}^{M} A_n \{Q_0\}_n^{(k)} e^{-\gamma_n z} \quad (8a)$$

where

$$\{\epsilon\}^{(k)T} = [\epsilon_{rr}, \epsilon_{\theta\theta}, \epsilon_{zz}, \gamma_{\theta z} = 2\epsilon_{\theta z}, \gamma_{rz} = 2\epsilon_{rz}, \gamma_{r\theta} = 2\epsilon_{r\theta}]^{(k)} \quad (8b)$$

The constitutive relations for the general cylindrically anisotropic lamina being used here are

$$\begin{Bmatrix} \sigma_{rr} \\ \sigma_{\theta\theta} \\ \sigma_{zz} \\ \sigma_{\theta z} \\ \sigma_{rz} \\ \sigma_{r\theta} \end{Bmatrix}^{(k)} = \begin{bmatrix} C_{11}^{(k)} & C_{12}^{(k)} & C_{13}^{(k)} & C_{14}^{(k)} & 0 & 0 \\ C_{12}^{(k)} & C_{22}^{(k)} & C_{23}^{(k)} & C_{24}^{(k)} & 0 & 0 \\ C_{13}^{(k)} & C_{23}^{(k)} & C_{33}^{(k)} & C_{34}^{(k)} & 0 & 0 \\ C_{14}^{(k)} & C_{24}^{(k)} & C_{34}^{(k)} & C_{44}^{(k)} & 0 & 0 \\ 0 & 0 & 0 & 0 & C_{55}^{(k)} & C_{56}^{(k)} \\ 0 & 0 & 0 & 0 & C_{56}^{(k)} & C_{66}^{(k)} \end{bmatrix} \begin{Bmatrix} \epsilon_{rr} \\ \epsilon_{\theta\theta} \\ \epsilon_{zz} \\ \gamma_{\theta z} \\ \gamma_{rz} \\ \gamma_{r\theta} \end{Bmatrix}^{(k)} \quad (9)$$

and relations between the C_{ij}, fiber angle in the lamina, and five independent material properties for transversely isotropic media can be found in Vinson and Chou.[4] Layers characterized as general anisotropic have coupled longitudinal and torsional motions.

Equation (7) is applied to each element in turn giving for the kth element

$$\{\delta A\}^T [Q]^{(k)T} \int_{r_b}^{r_f} [N]^{*T} [C]^{(k)*} ([b][Q']^{(k)} + [a][Q]^{(k)}) \{A\} r \, dr = 0 \quad (10a)$$

where

$$[Q]^{(k)} = [\{Q_0\}_1^{(k)} \{Q_0\}_2^{(k)} \cdots \{Q_0\}_M^{(k)}] \quad (10b)$$

$$[Q']^{(k)} = [-\gamma_1 \{Q_0\}_1^{(k)} - \gamma_2 \{Q_0\}_2^{(k)} \cdots - \gamma_M \{Q_0\}_M^{(k)}] \quad (10c)$$

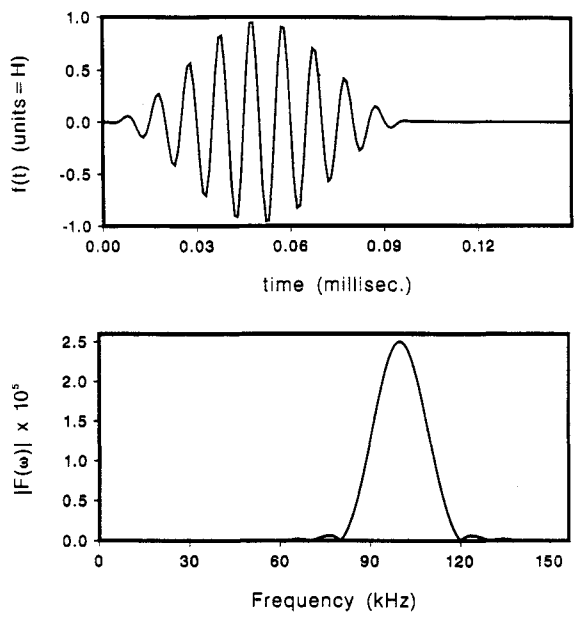

Fig. 2 Time domain and frequency spectrum for "modified toneburst" (100 μs duration; 100 kHz center frequency).

The modal amplitude vector $\{A\}$ is

$$\{A\}^T = [A_1 A_2 \cdots A_M] \quad (10d)$$

and

$$[N]^* = \begin{bmatrix} 0 & \eta_1 & 0 & 0 & \eta_2 & 0 & 0 & \eta_3 & 0 \\ \eta_1 & 0 & 0 & \eta_2 & 0 & 0 & \eta_3 & 0 & 0 \end{bmatrix} \quad (10e)$$

$$[C]^{(k)*} = \begin{bmatrix} C_{14}^{(k)} & C_{24}^{(k)} & C_{34}^{(k)} & C_{44}^{(k)} & 0 & 0 \\ 0 & 0 & 0 & 0 & C_{55}^{(k)} & C_{56}^{(k)} \end{bmatrix} \quad (10f)$$

Contributions to a consistent nodal force vector from the kth element are obtained from Eq. (10a) as

$$\left\{ \int_{r_b}^{r_f} [N]^{*T} [C]^{(k)*} [b] r \, dr [Q']^{(k)} + \int_{r_b}^{r_f} [N]^{*T} [C]^{(k)*} [a] r \, dr [Q]^{(k)} \right\} \{A\} = \{F\}^{(k)} \quad (11a)$$

where

$$\{F\}^{(k)T} = [F_{r_b} F_{\theta_b} 0 F_{r_m} F_{\theta_m} 0 F_{r_f} F_{\theta_f} 0]^{(k)} \quad (11b)$$

is the nodal force vector. The integrals of Eq. (11a) can be evaluated exactly given the element geometry (inner and outer radii r_b and r_f). Equation (11a) gives a $9 \times M$ matrix for each element with rows 3, 6, and 9 entirely zero. Assembly of a global representation of $\{F\}$ is done in the usual manner.

The nonhomogeneous displacement part of the boundary condition is obtained again from Eqs. (6a) and (6b) setting the $(3xi - 2)$ and $(3xi - 1)$ rows of all $\{Q_0\}_n$ to zero, where i ranges from 1 to P (number of nodes). The resulting displacement boundary condition equation is then used together with the force boundary condition equation derived from Eqs. (11a) and (11b).

For specified ω, solution of either boundary value problem yields the frequency domain impulse response $G(\omega)$ for any of the displacements, strains, or stresses of interest at that frequency as given by Eqs. (4), (8a), and (9), respectively. As mentioned earlier, the prescribed nonzero boundary condition of a uniform axial displacement is a function of time, $u_z(z = 0,t) = f(t)$. The time domain response for any field variable, say $x(t)$, may be written as a convolution between the time domain impulse response $g(t)$ and the excitation that is here the prescribed displacement $f(t)$:

$$x(t) = \int_0^t f(\lambda) g(t - \lambda) \, d\lambda \quad (12)$$

Convolution in the time domain implies multiplication in the frequency domain. The frequency domain transform of the field variable $x(t)$ is then given as $X(\omega) = G(\omega)F(\omega)$. Therefore, once the frequency domain impulse response $G(\omega)$ has been determined, we merely need to multiply by the forward Fourier transform $F(\omega)$ of the excitation or prescribed displacement $f(t)$. Subsequently, an inverse fast Fourier transform (FFT) will give the time response $x(t)$ of the field variable of interest. The impulse reponse is determined at discrete frequencies over a sufficient range so that the significant part of the spectrum of the product of $G(\omega)$ and $F(\omega)$ is included in the inverse transform computation.

Some additional care is required to avoid errors that may occur due to numerical ill-conditioning in the impulse response data. Rapid variations in both amplitude and phase of the impulse response near cutoff frequencies can cause spurious waves to appear in the predicted time response before the first arrival of the waveform should occur. It was empirically found that by increasing the frequency resolution such that $z_0/c_{g\min} < 1/(2\Delta f)$, these spurious waves were removed. Here, Δf is the frequency increment in the inverse FFT data, z_0 is the axial location where the impulse response is being computed,

and $c_{g\min}$ is the minimum group velocity calculated for any mode over the frequency range considered. An alternative and more efficient technique was setting the amplitude to zero for any mode with group velocity c_g such that $z_0/c_g > 1/(2\Delta f)$. Both techniques are effective in removing the spurious waves and yield essentially the same response.

Ply Lay-Up and Material Properties

Specifically, we will be considering "specially orthotropic" tubes with even numbers of equal thickness laminas stacked symmetrically with respect to the midsurface of the tube with alternating plus and minus fiber angles. The particular tube ply lay-up considered here is $[15, -15]_s^6$ as shown in Fig. (1b). The wall thickness to midsurface radius ratio used was $H/R = 1/10$ and a wall thickness of $H = 0.1$ in. The material properties for uniaxial graphite fiber reinforced epoxy, as given by Sun and Whitney,[5] are $E_L = 20 \times 10^6$ psi (138 GPa); $E_T = 10^6$ psi (6.9 GPa); $G_{TT} = 0.5 \times 10^6$ psi (3.45 GPa); $G_{LT} = 0.6 \times 10^6$ psi (4.14 GPa); $\nu_{LT} = 0.25$ where L signifies the fiber direction and T the transverse direction.

Results and Discussion

The tube end axial displacement for each type of boundary condition is in the form of a pulse or small duration disturbance. Two types of such pulse excitations with considerably different frequency content will be examined here. The first of these is a "modified toneburst," with 10 cycles of a sine wave superimposed on an inverted 100 μs duration (τ) Hanning window. Time domain and frequency spectra plots of this pulse are shown in Fig. 2. The time varying function representing this pulse is given by

$$u_z(z=0,t) = f(t) = -\frac{H}{2}\left[1-\cos\left(\frac{2\pi t}{\tau}\right)\right]\sin\left(\frac{2\pi t}{\tau/10}\right) \quad \text{for } 0 \le t \le \tau \qquad (13)$$

$$= 0, \quad \text{otherwise}$$

The second pulse considered is a 100 μs duration (τ) Hanning pulse with time domain and frequency spectra plots shown in

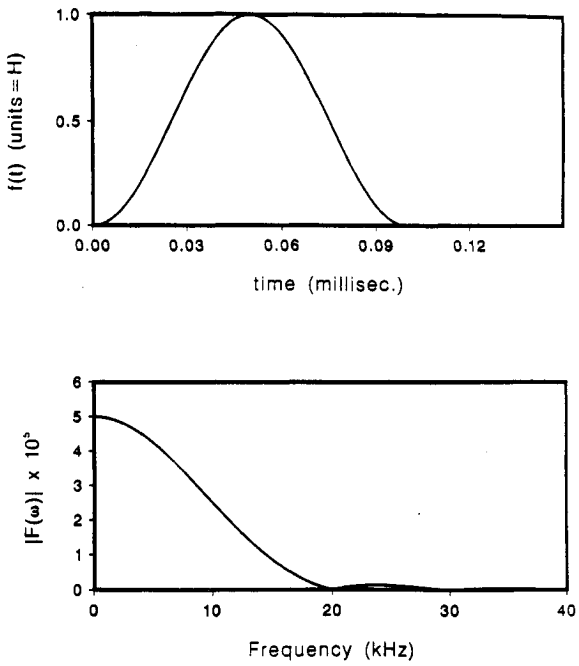

Fig. 3 Time domain and frequency spectrum for 100 μs Hanning pulse.

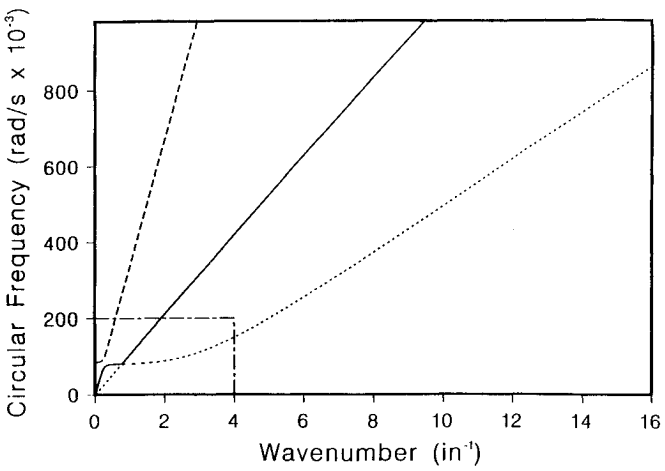

Fig. 4a Wavenumber vs angular frequency: ————, branch 1; ----------, branch 2; ————, branch 3.

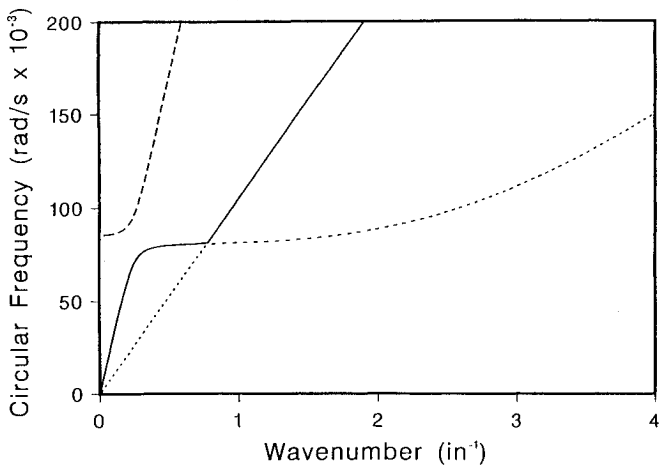

Fig. 4b Expanded view of sectioned area in Fig. 4a: ————, branch 1; ----------, branch 2; ————, branch 3.

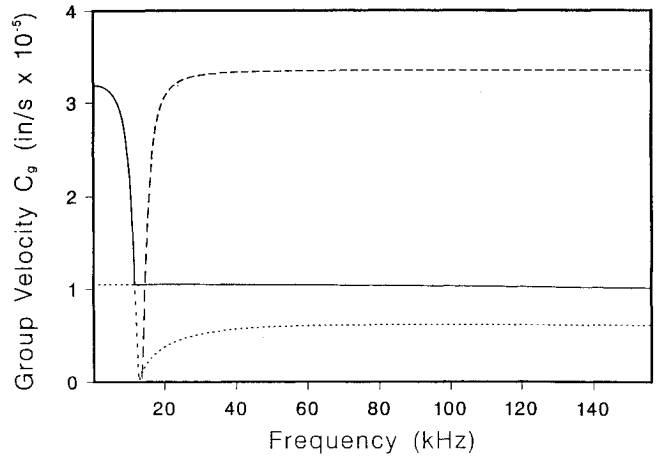

Fig. 4c Frequency vs group velocity: ————, branch 1; ----------, branch 2; ————, branch 3.

Fig. 3. The time varying function for the Hanning pulse is given by

$$u_z(z=0,t) = \frac{H}{2}\left[1-\cos\left(\frac{2\pi t}{\tau}\right)\right], \quad \text{for } 0 \le t \le \tau \qquad (14)$$

$$= 0, \quad \text{otherwise}$$

The frequency content of the modified toneburst is banded, centered at 100 kHz, whereas the content of the Hanning pulse is essentially insignificant beyond approximately 30 kHz as shown in Figs. 2 and 3. For pulses such as these, involving frequencies that are low relative to those used in most ultrasonic applications, fewer elements are required to obtain convergence of the solution. Here, 12 elements (one for each lamina) were found to be adequate.

It is essential to examine and understand the dispersion curves for the tubes considered within the ranges of frequency of these excitations before we relate the dispersion and boundary conditions to the observed time responses. For tubes of the dimensions considered here, any tube with ply lay-up of the form $[15, -15]_s^n$ will have essentially the same dispersion curves in the frequency range being considered (to 150 kHz),

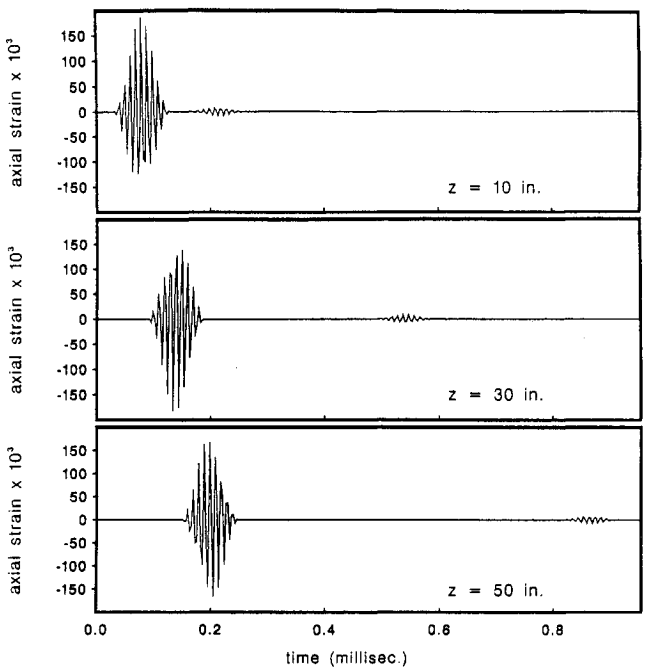

Fig. 5a Axial strain time responses at three stations for B.C.I and modified toneburst excitation.

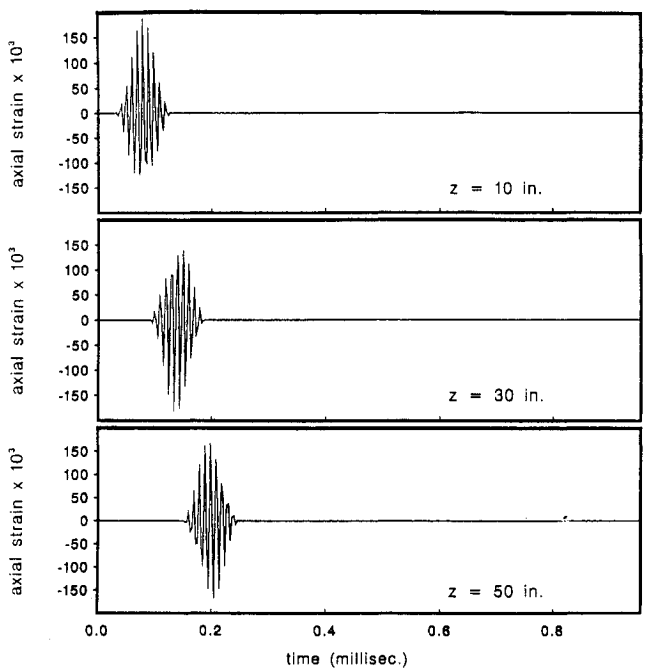

Fig. 5b Axial strain time responses at three stations for B.C.II and modified toneburst excitation.

although in the higher frequency range the modal behavior may differ according to the value of n as discussed in Kohl et al.[2] A frequency spectrum (ω vs ξ graph) is shown in Fig. 4a. The sectioned area in Fig. 4a is shown in expanded view in Fig. 4b. Note that branches 1 and 2 appear as if they should cross where these branches come together at a circular frequency of approximately 80,000 rads/s. In fact, these branches do not cross as shown in Figs. 4a and 4b. The noncrossing of the branches is due to the coupling between longitudinal and torsional motions. Although the branches do not cross, there is an interchange of mode shapes between the branches. Because this interchange occurs over a very small span of frequency (approximately 2 Hz), the longitudinal/torsional coupling is physically unimportant at these relatively low frequencies, as discussed in greater detail in Kohl et al.[2] Aside from the aforementioned small span of frequency in which the mode interchange occurs, the mode shapes that occur at a particular frequency are analogous to those that occur in orthotropic media where torsional and longitudinal motions are uncoupled. Consequently, for clarity in the remainder of this paper, we will refer to the segment of branch 1 before the close approach of branches 1 and 2, and the segment of branch 2 after this close approach as the first longitudinal mode. This is done because the mode shapes associated with these segments of branches 1 and 2 are analogous to the mode shapes for the first longitudinal mode in an orthotropic tube. Similarly, the segments of branch 2 before and branch 1 after this close approach will be referred to as the first torsional mode.

Given the relation that the group velocity c_g may be written $c_g = d\omega/d\xi$, it is seen that the group velocity for an individual mode is the slope of the frequency spectra line of that mode at a particular frequency. Since the component modes of a disturbance propagate at the individual group velocities, a tube will exhibit dispersion if there are modes contributing significantly to the response at frequencies where the group velocities change significantly.

Figure 4c shows a plot of group velocity vs frequency. Since the first torsional mode is relatively uninvolved in the response, due to the weakness of the torsional/longitudinal motion coupling in this frequency region, only for a narrow band of frequency near 13 kHz where there exist rapid variations in group velocity, one would expect to see pronounced dispersive effects. As can be seen very clearly in Fig. 4c, this band of highly dispersive behavior is centered around the cutoff frequency of the second propagating longitudinal mode.

Figures 5 and 6 show time domain behavior of axial strain and radial displacement, respectively, for the $[15, -15]_s^6$ tube due to the modified toneburst excitation. The responses are shown for stations at three different axial locations on the tube outer surface for each boundary condition. In light of the preceding discussion regarding dispersive effects and the frequency spectrum of the excitation in Fig. 2, it is not unexpected that little dispersion will be evident. Referring to Figs. 5a and 5b, the pulse remains "undistorted" with variation in the axial location of the receiver for both boundary conditions. With increasing distance from the tube end, the pulse arrives after more elapsed time.

There may be discerned, however, small "bumps" in the axial strain responses of Fig. 5a for B.C.I, after the passage of the primary disturbance, that are barely visible in the responses for B.C.II in Fig. 5b. This may be explained by examining the radial displacement time response plots of Figs. 6a and 6b. Here, behavior analogous to those of Fig. 5 are seen, but the small bumps occurring for B.C.I in Fig. 5a are now a well-defined disturbance in Fig. 6a. The explanation for these more slowly propagating disturbances for B.C.I is the presence of a second significant contributing mode. The second mode is present because of the form of the boundary condition and the shapes of the contributing modes. The "dominant" part of either boundary condition may be thought of as the required axial displacement. Generally, at a given frequency, the mode with a shape that is capable of

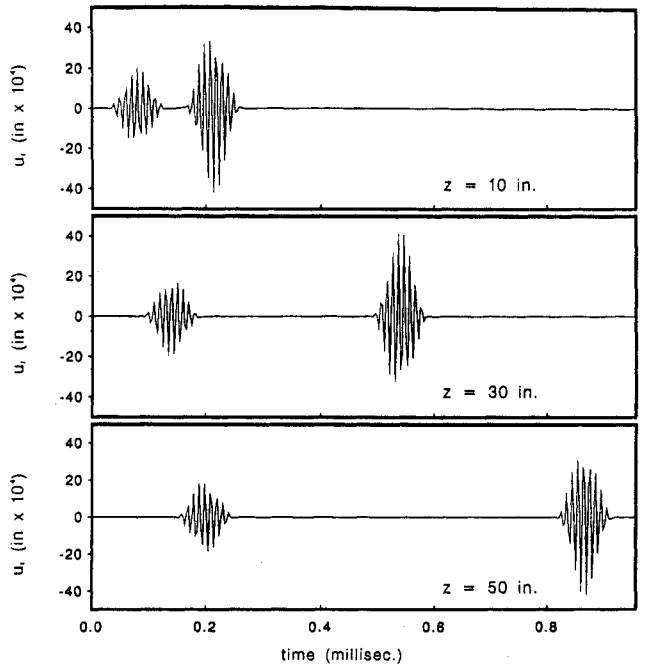

Fig. 6a Radial displacement time responses at three stations for B.C.I and modified toneburst excitation.

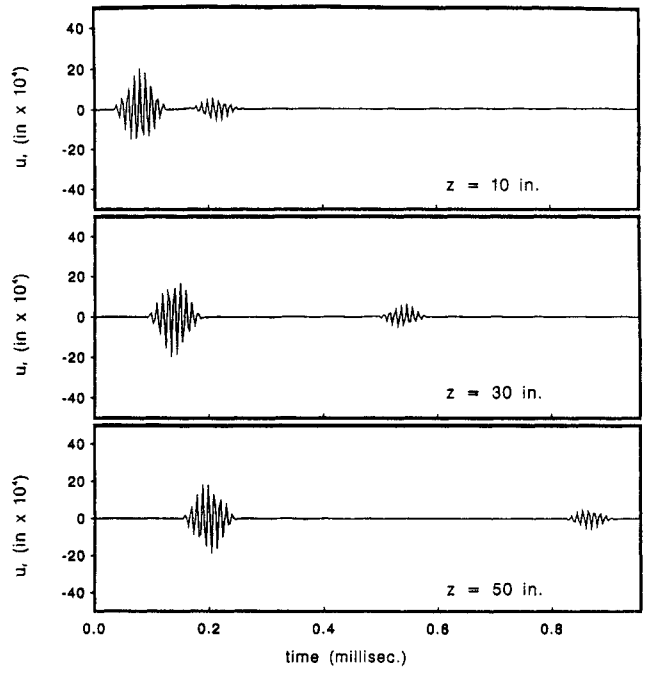

Fig. 6b Radial displacement time responses at three stations for B.C.II and modified toneburst excitation.

satisfying this part of the boundary condition propagates at the highest velocity. However, within this mode shape, there is a radial displacement component associated with the predominantly axial motion. The imposition of B.C.I, with prescribed zero radial displacement, tends to cause a canceling contribution from a second propagating mode, which possesses predominantly radial motion. This mode propagates at lower velocity as can be seen by examining Fig. 4c. The small axial component of this second slower mode is responsible for the bumps in Fig. 5a for B.C.I. There is really no dispersion occurring here, but rather two modes propagating nondispersively at different velocities.

The situation for disturbances engendered by the Hanning pulse excitation is considerably different. Because the frequency spectrum of this excitation has much more significant amplitude in a frequency range where dispersion is present, as can be seen by comparing Figs. 3b and 4c, it is to be expected that dispersive effects will be more prevalent in this case compared with those from the modified toneburst. Figures 7 and 8 show axial strain and radial displacement time responses, respectively, for the Hanning pulse excitation. The presence of dispersive effects are easily seen in the distortion of the form of the disturbance with varying axial location.

Although the overall time response is considerably more complex for the dispersive case, some general similarities to the relatively nondispersive modified toneburst responses should be noted with regard to the differences in boundary conditions. Note that the "short time" response at a given axial position is basically identical for the two boundary con-

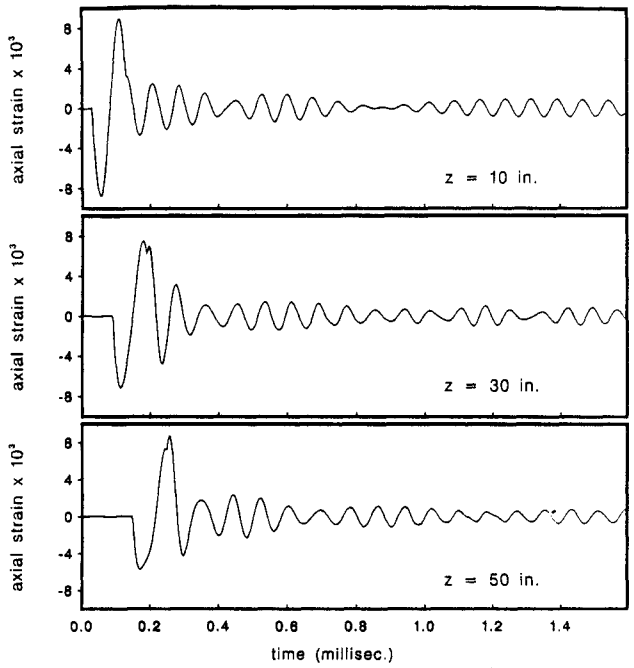

Fig. 7a Axial strain time responses at three stations for B.C.I and 100 μs excitation.

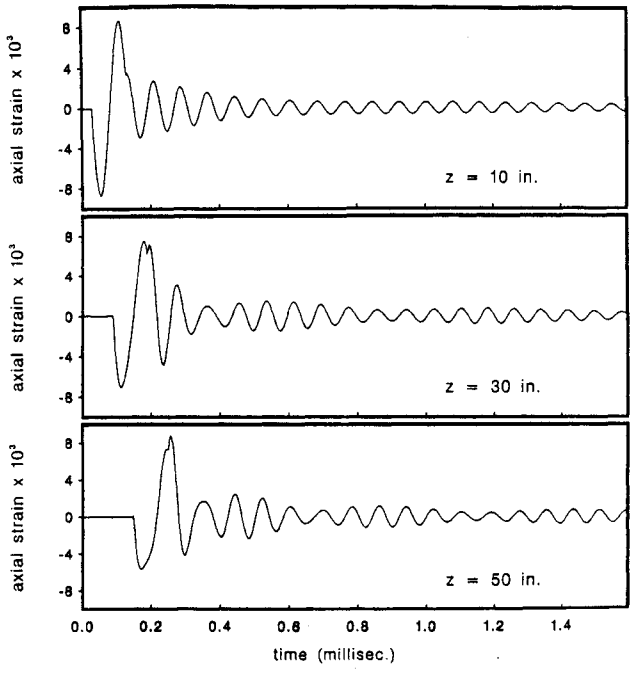

Fig. 7b Axial strain time responses at three stations for B.C.II and 100 μs excitation.

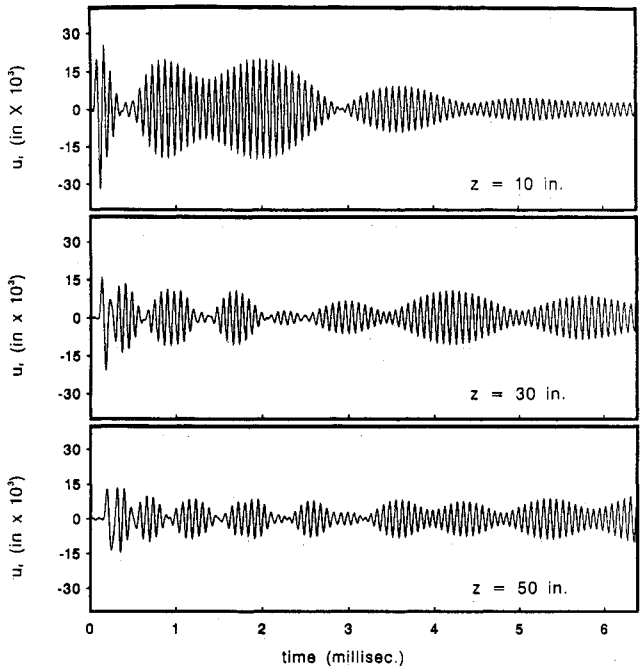

Fig. 8a Radial displacement time responses at three stations for B.C.I and 100 μs excitation.

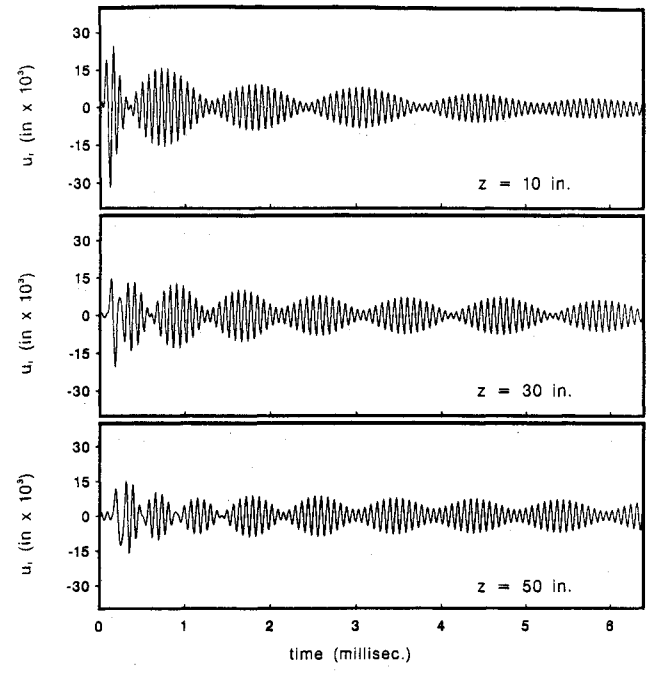

Fig. 8b Radial displacement time responses at three stations for B.C.II and 100 μs excitation.

ditions, whereas the "long time" responses are dissimilar. Reference to "short" vs "long" time must be taken in the context of the axial position. As we increase the axial coordinate, the short time is extended to greater elapsed time. By analogy to prior observations, this indicates that contributions from modes with higher speeds of propagation with principally axial displacement component are basically equivalent in both cases. More slowly propagating modes with principally radial displacement component are increasingly involved when B.C.I is applied, as may be seen in the significantly greater

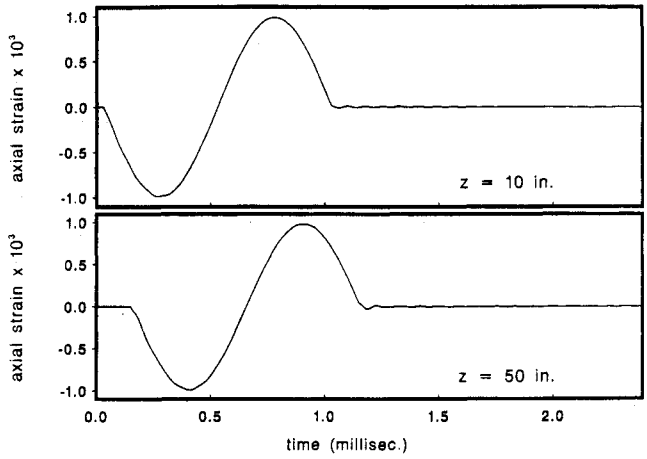

Fig. 9 Axial strain time responses at two stations for B.C.I and 1.0 ms excitation.

radial displacement magnitudes at longer times for B.C.I in Fig. 8a than for B.C.II in Fig. 8b.

It should also be noted that dispersive effects can be avoided by limiting the frequency content of the excitation to frequencies significantly below the band where variations in group velocity are evident. As an illustration, Fig. 9 shows axial strain time responses for B.C.I when a 1 ms Hanning pulse is applied to the tube end. Dispersive effects are nearly eliminated due to the lower frequency content of longer duration Hanning pulses.

Conclusion

A wave propagation based finite element method has been used to obtain dispersive modes of propagation for axisymmetric motion in radially inhomogeneous laminated composite tubes. Boundary conditions were then imposed on the tube end to solve for the modal amplitudes. The boundary conditions applied were a time varying uniform axial displacement of the tube end together with either zero radial and circumferential displacements or zero shear stresses at the tube end. Knowledge of the dispersion relations, modes, and modal amplitudes gave a frequency domain impulse response solution in a semi-infinite tube for any of the displacements, strains, or stresses at a specified axial and radial location. For a given time dependent end axial displacement, a fast Fourier transform was used to obtain the time response of the displacement, strain, or stress of interest.

In the particular tube considered here and for the frequency range assumed, the time response due to more rapidly propagating, predominantly axial displacement component modes was unaffected by the changes in the boundary conditions. The changes in the boundary conditions were found to significantly affect contribution from more slowly propagating, predominantly radial modes. The zero radial and circumferential displacement condition tended to increase involvement of these modes.

The extent of dispersion observed was also examined in relation to the frequency content of the excitation. It was predicted by examination of the dispersion curves and corroborated by the numerical modeling of the time response that dispersive effects were limited to certain frequency bands. By applying a banded excitation with frequency content predominantly well above the cutoff frequency of the second longitudinal mode and below the cutoff of higher modes, dispersion was reduced. Conversely, an excitation with significant content near the cutoff of the second longitudinal mode was seen to produce a highly dispersive disturbance. Excitations with frequency content significantly below the cutoff of the second longitudinal mode also exhibited little dispersion.

Appendix

$$[N(r)] = \begin{bmatrix} \eta_1 & 0 & 0 & \eta_2 & 0 & 0 & \eta_3 & 0 & 0 \\ 0 & \eta_1 & 0 & 0 & \eta_2 & 0 & 0 & \eta_3 & 0 \\ 0 & 0 & \eta_1 & 0 & 0 & \eta_2 & 0 & 0 & \eta_3 \end{bmatrix}$$

$$\eta_1(r) = 1 - 3\hat{r} + 2\hat{r}^2, \quad \eta_2(r) = 4\hat{r} - 4\hat{r}^2, \quad \eta_3(r) = -\hat{r} + 2\hat{r}^2$$

$$[m] = \int_r \rho^{(k)}[N]^T[N]r \, dr, \quad [k_2] = \int_r [b]^T[C^{(k)}][a]r \, dr$$

$$[k_1] = \int_r [b]^T[C^{(k)}][b]r \, dr, \quad [k_3] = \int_r [a]^T[C^{(k)}][a]r \, dr$$

$$[a] = \begin{bmatrix} \frac{\partial \eta_1}{\partial r} & 0 & 0 & \frac{\partial \eta_2}{\partial r} & 0 & 0 & \frac{\partial \eta_3}{\partial r} & 0 & 0 \\ \frac{\eta_1}{r} & 0 & 0 & \frac{\eta_2}{r} & 0 & 0 & \frac{\eta_3}{r} & 0 & 0 \\ 0 & 0 & 0 & 0 & 0 & 0 & 0 & 0 & 0 \\ 0 & 0 & 0 & 0 & 0 & 0 & 0 & 0 & 0 \\ 0 & 0 & \frac{\partial \eta_1}{\partial r} & 0 & 0 & \frac{\partial \eta_2}{\partial r} & 0 & 0 & \frac{\partial \eta_3}{\partial r} \\ 0 & \left(\frac{\partial \eta_1}{\partial r} - \frac{\eta_1}{r}\right) & 0 & 0 & \left(\frac{\partial \eta_2}{\partial r} - \frac{\eta_2}{r}\right) & 0 & 0 & \left(\frac{\partial \eta_3}{\partial r} - \frac{\eta_3}{r}\right) & 0 \end{bmatrix}$$

$$[b] = \begin{bmatrix} 0 & 0 & 0 & 0 & 0 & 0 & 0 & 0 & 0 \\ 0 & 0 & 0 & 0 & 0 & 0 & 0 & 0 & 0 \\ 0 & 0 & \eta_1 & 0 & 0 & \eta_2 & 0 & 0 & \eta_3 \\ 0 & \eta_1 & 0 & 0 & \eta_2 & 0 & 0 & \eta_3 & 0 \\ \eta_1 & 0 & 0 & \eta_2 & 0 & 0 & \eta_3 & 0 & 0 \\ 0 & 0 & 0 & 0 & 0 & 0 & 0 & 0 & 0 \end{bmatrix}$$

Acknowledgment

This work was supported by NASA Grant NAGW-1388.

References

[1]Nelson, R. B., Dong, S. B., and Kalra, R. D., "Vibrations and Waves in Laminated Orthotropic Circular Cylinders," *Journal of Sound and Vibration,* Vol. 18, 1971, pp. 429–444.

[2]Kohl, T., Datta, S. K., Shah, A. H., and Rattanawangcharoen, N., "Mode-Coupling of Waves in Laminated Tubes," *Journal of Composite Materials* (to be published).

[3]Huang, K. H., and Dong, S. B., "Propagating Waves and Edge Vibrations in Anisotropic Composite Cylinders," *Journal of Sound and Vibration,* Vol. 96, 1984, pp. 363–379.

[4]Vinson, J. R., and Chou, T. W., *Composite Materials and Their Use in Structures,* Applied Science Publishers, London, 1975, pp. 206–223.

[5]Sun, C. T., and Whitney, J. M., "Axisymmetric Vibrations of Laminated Composite Cylindrical Shells," *Journal of the Acoustical Society of America,* Vol. 55, 1974, pp. 1238–1246.